Effect of different solvents on the structural and optical properties of zinc oxide thin films for optoelectronic applications

K.L. Foo*, M. Kashif, U. Hashim, Wei-Wen Liu

Nano Biochip Research Group, Institute of Nano Electronic Engineering (INEE), Universiti Malaysia Perlis (UniMAP), 01000 Kangar, Perlis, Malaysia

Abstract

Zinc oxide (ZnO) seed solutions were prepared using 4 different solvents, namely, methanol (MeOH), ethanol (EtOH), isopropyl alcohol (IPA) and 2-methoxyethanol (2-ME). The prepared seed solutions were used to synthesize ZnO thin films using a low-cost sol–gel spin-coating method. The effect of different solvents on the structural and optical properties of ZnO thin films was investigated by field emission scanning electron microscopy (FESEM), atomic force microscopy (AFM), and an ultraviolet–visible–near infrared spectrophotometer (UV–vis–NIR). The images obtained in the FESEM and AFM showed that the thin film prepared using 2-ME has the smallest grain size. Moreover, the X-ray diffraction (XRD) results showed that the synthesized ZnO films are polycrystalline with preferred orientation along the (002) plane, whereas the IPA-derived films have a preferred orientation on (101) plane. The ZnO thin film synthesized with 2-ME has the highest transmittance (> 90%), lowest surface roughness of 3.131 nm and highest band gap energy of 3.28 eV. The experimental data are in agreement with the calculated results by specific models of refractive index.
© 2013 Elsevier Ltd and Techna Group S.r.l. All rights reserved.

Keywords: Zinc oxide; Solvents; Optical; Structural; Sol–gel

1. Introduction

Zinc Oxide (ZnO) is a well-known semiconductor that has wide direct band-gap (3.37 eV) at room temperature and large free excitation binding energy (60 meV). ZnO has high thermal stability, highly crystalline hexagonal structure, and high mechanical strength, which make it suitable for use as an electronic material in various fields such as bio-molecule sensor [1,2], ultraviolet (UV) detector [3], light-emitting diode [4], chemical and gas sensor [5,6], solar cell [7,8], and optoelectronic [9].

The nanoparticles in ZnO thin films act as a seeding layer in the formation of other nanostructures, such as nanowires [1,10], nanopores [11], nanorods [12], nanobelts [13], nanorings [14], nanocables [15], nanotubes [16,17], nanocolumns [18], nanocombs [19], and nanoneedles [20]. Therefore, ZnO

has an important function in the growth of these nanostructures. Various methods are used in the deposition of ZnO thin films, such as spin-coating method [21,22], radio frequency sputtering [23], pulsed laser deposition, metal–organic chemical vapor deposition (MOCVD) [24], physical vapor deposition [25], spray pyrolysis [26], and ink-jet printing [27].

Previous research has shown that high-quality and uniform ZnO thin films are produced when deposited by sputtering methods and vapor phase techniques like MOCVD [21,28–30]. However, these techniques require complex and expensive experimental setups [28]. Therefore, a low-cost and simplified fabrication route for depositing ZnO thin films by sol–gel method is developed. This technique provides several advantages in terms of reliability, repeatability, low temperature, and ease of composition control. The optical, chemical, and structural properties of ZnO thin films are strongly dependent on precursors, solvents, temperature, and time. Thus, studying the effect of different solvents in the structural, morphological, and optical properties of ZnO thin films is important. Previous researchers have studied the

*Corresponding author. Tel.: +60 49798580/8581, +60 128913635; fax: +60 49798578.

E-mail address: elitefoo@yahoo.com (K.L. Foo).

effect of different solvents using isopropyl alcohol (IPA), methanol (MeOH), and 2-methoxyethanol (2-ME) [31]. However, few studies have published reports on ethanol (EtOH)-based ZnO thin films [32].

In this study, a low-cost spin-coating method was used in the synthesis of ZnO thin films on silicon oxide (SiO_2) substrate using different solvents. The aim of this current study is to investigate the effect of different solvents on the material properties. To the best of our knowledge, no published literature has analyzed the effect of different solvents on ZnO thin films and compared them with the specific models of refractive index.

2. Experimental

ZnO seed solution was prepared using zinc acetate dihydrate [$Zn(CH_3COO)_2 \cdot 2H_2O$] (98%; Sigma-Aldrich), which was free from chlorine ions and used as a precursor. Different solvents were used without further purification, namely, MeOH (99.8%; Merck), EtOH (99.99%; J.T. Baker), IPA (99.5%; Sigma-Aldrich) and 2-ME (99.8%; Sigma-Aldrich). Monoethanolamine (MEA; 99%; Merck) was used as a stabilizer. To prepare ZnO seed solutions, 4.39 g of Zn $(CH_3COO)_2 \cdot 2H_2O$ was dissolved in 100 ml of different solvents. The concentration of ZnO in all of the solutions was kept constant at 0.2 M. The mixed solution was then vigorously stirred with a magnetic stirrer at 60 °C for 30 min. MEA was added drop by drop to the milky ZnO solution with constant stirring at 60 °C for 2 h. Finally, homogenous and transparent ZnO solutions were obtained. The prepared solutions were stored at room temperature for 24 h. The process flow in the preparation of ZnO seed solution is shown in Fig. 1.

P-type silicon (100) wafer was used as a substrate to deposit the thin films. Three layers of ZnO thin films were deposited using the process shown in Fig. 1. Prior to the deposition process, the silicon substrates were ultrasonically cleaned with acetone and IPA. Buffer oxide etch solution was used to remove the native oxide layer from the substrates which were finally rinsed with deionized water. A SiO_2 oxide layer with ~180 nm thickness was grown on the cleaned substrate using wet oxidation process. In this process, the cleaned substrate was placed in the middle of the furnace at 1000 °C, with the water vapor continuously flowing into the tube furnace at a rate of 10 L/min for 1 h.

The stock solutions were spin coated on the pre-cleaned SiO_2/Si substrates at a spin rate of 3000 rpm for 20 s using a conventional photoresist spin coater. The coated layers were dried on a hot plate at 150 °C for 10 min. The coating-to-drying process of all the solvent-derived films was repeated 3 times. Using a conventional furnace, the coated films were annealed at 500 °C for 2 h in air.

The morphology of the ZnO thin films was examined using field emission scanning electron microscopy (FESEM; Carl Zeiss AG-ULTRA 55, Gemini). Crystallization and microstructures of the ZnO thin films were characterized using an atomic force microscope (AFM; SPA400-SPI3800, Seiko
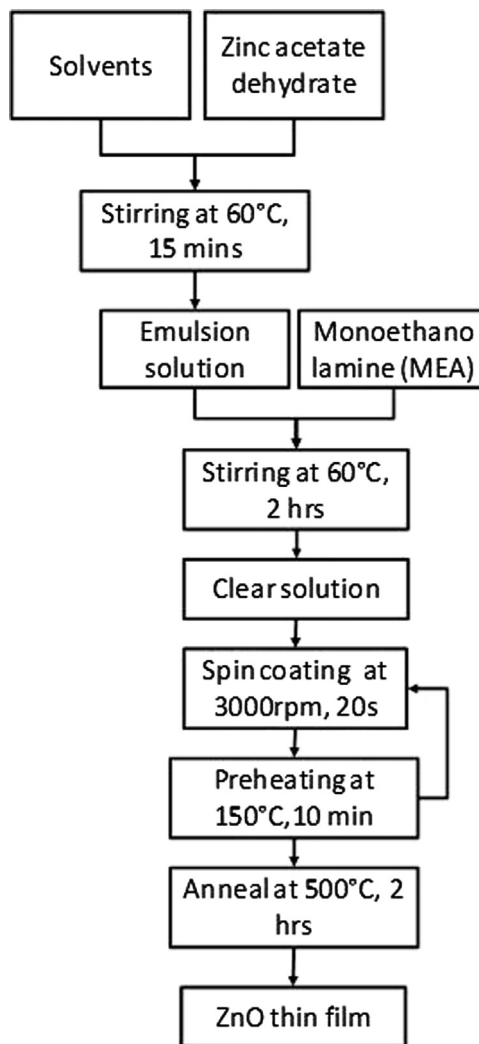

Fig. 1. ZnO thin films preparation process flow.

Instruments Inc., Japan) and X-ray diffraction (XRD; Bruker D8) with CuKα radiation from 30° to 70° 2θ operated at 40 kV and 40 mA. The elemental stretching vibration was analyzed using Fourier transform infrared (FTIR; Perkin-Elmer Spectrum 400 spectrometer) within the range of 400–2000 cm^{-1}. Optical transmittance measurements were carried out using an ultraviolet–visible–near infrared spectrophotometer (UV–vis–NIR; Perkin-Elmer Lambda 950) with a slit width of 2 nm at normal incidence. All measurements were carried out at room temperature.

3. Results and discussion

The surface morphology of the ZnO thin films coated by different solvents is shown in Fig. 2. The obtained FESEM images show that all the ZnO thin films consist of nanoparticles with diameters less than 50 nm. ZnO crystalline grains with hexagonal morphology consistently appear on the substrate surfaces. The different degrees of brightness of the grains indicate the presence of multiple layers of ZnO on the substrates. The brighter grains represent the upper layer of
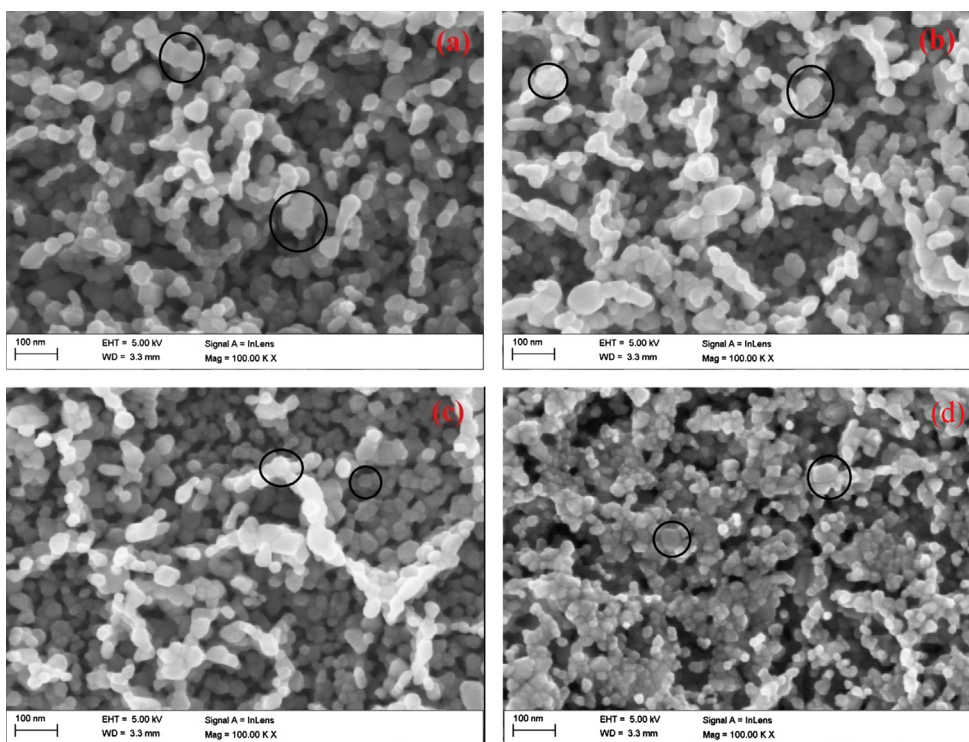
Fig. 2. FESEM micrographs of ZnO nanoparticles prepared with different solvents: (a) MeOH, (b) EtOH, (c) IPA, and (d) 2-ME.

the thin films and the darker grains represent the lower layer of the thin films.

To study the surface morphology and roughness of ZnO thin films with different solvents, AFM was employed to image the ZnO thin films over a 500 nm^2 area. The top and three-dimensional views of the ZnO thin films with different solvents are demonstrated in Figs. 3 and 4, respectively. The results show that the different solvents used in the preparation of ZnO solution strongly affect the properties of the ZnO thin film surface. The surface roughness, grain size, and RMS values are presented in Table 1. The tabulated values of AFM data show that the ZnO thin film synthesized using 2-ME exhibited the smallest grain size, RMS, and surface roughness values of 58.14, 4.233, and 3.131 nm, respectively. The ZnO thin film synthesized using EtOH solvent has the largest grain size, RMS, and surface roughness values of 129.1, 9.0243, and 6.617 nm, respectively.

The microstructure and crystalline phase of the prepared ZnO thin films were examined using XRD. The XRD pattern of the ZnO thin films is shown in Figs. 4 and 5. All the diffraction peaks are in accordance to the standard card (JCPDS36-1451). The XRD patterns show that the synthesized films have a polycrystalline phase with a hexagonal wurtzite structure, as reported in the literature [33].

From the XRD patterns, the ZnO solution synthesized with MeOH, EtOH, and 2-ME exhibits the highest intensities of crystal growth orientation on the (002) plane, which is located at 34.5°. However, the IPA solvent exhibits the highest intensities of crystal growth orientation on the (101) plane, which is located at 36.3°. The presence of a high-intensity

peak on the (101) plane of IPA may be attributed to the low annealing temperature used to achieve crystal growth orientation on the (002) plane [34]. Previous researchers have reported that annealing the IPA solvent-based ZnO thin films at 450 °C for 1 h exhibited the same trend [35].

The average crystallite size of the ZnO thin films was estimated using Scherrer's formula [36]

$$D = \frac{\kappa \lambda}{\text{FWHM } \cos \theta} \qquad (1)$$

where κ is the Scherrer constant dependent on crystallite shape and can be considered as 0.9 [37,38], λ is the incident X-ray wavelength, FWHM is the full-width at half-maximum of the respective peak, and θ represents the diffraction peak angle. The ZnO thin films synthesized with MeOH, EtOH, and 2-ME exhibit the highest XRD diffraction peaks on the (002) plane, so the crystallite sizes of the ZnO are highlighted on the (002) plane. ZnO thin films synthesized with IPA exhibit the highest XRD diffraction peak on the (101) plane. Therefore, the crystallite size along this plane was calculated. The calculated crystallite size using Eq. (1) is presented in Table 1. The average crystal size of the ZnO thin films ranges from 19.12 nm to 22.84 nm. The result shows that the ZnO thin films prepared using 2-ME produce the smallest crystallite size (19.12 nm). However, the ZnO thin films prepared using EtOH produce the largest crystallite size (22.84 nm). The largest crystalline size displayed by the film prepared using EtOH solvent can be attributed to higher viscosity of EtOH compared with other solvents. The results are in accordance with the AFM findings.
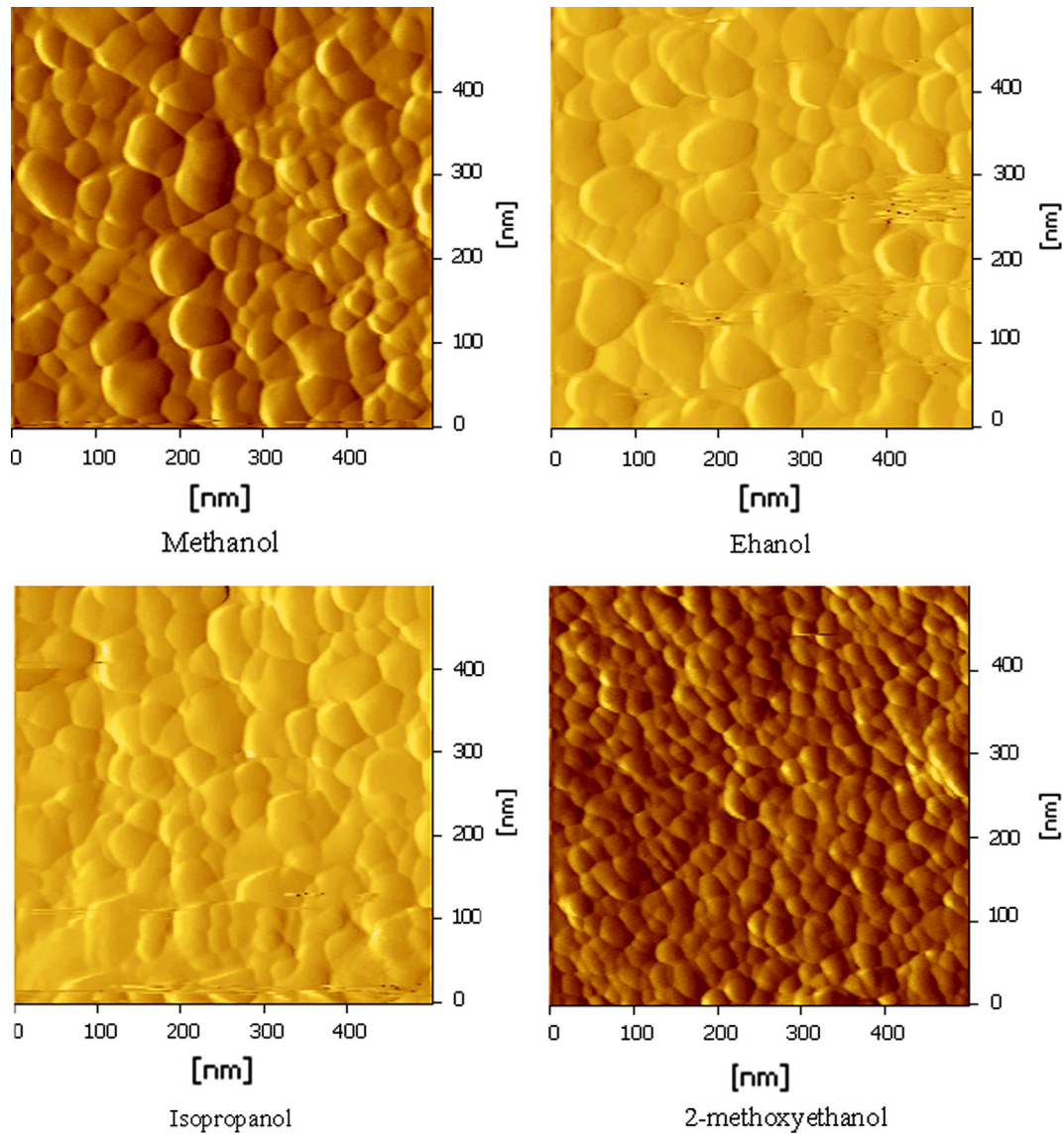
Fig. 3. AFM images of ZnO thin films synthesized with different solvents.

Table 1
Measured structural and optical properties of ZnO thin films using AFM and UV–vis for different solvents.

Solvent	Surface roughness (nm)	Grain size (mean diameter) (nm)	RMS (nm)	Peak vs. valley (P–V) (nm)	Band-gap (eV)
MeOH	5.194	91.37	6.615	44.78	3.25
EtOH	6.617	129.1	9.024	106	3.27
IPA	6.017	87.91	7.478	38.03	3.28
2-ME	3.131	58.14	4.233	35.82	3.28

The lattice constants 'a' and 'c' were calculated using the equations [39]

$$a = \sqrt{\frac{1}{3} \frac{\lambda}{\sin\theta}} \qquad (2)$$

$$c = \frac{\lambda}{\sin\theta} \qquad (3)$$

where λ is the X-ray wavelength of the incident CuK$_\alpha$ radiation (0.154056 nm). The calculated lattice constants 'a' and 'c' of the ZnO thin films prepared using different solvents are shown in Table 2. Higher values for 'a' and 'c' were found for the ZnO film prepared by IPA solvent ('a' = 3.23877 Å and 'c' = 5.20987 Å), which were closest to the pure bulk ZnO.

Chemical bonding that appeared in the prepared ZnO thin films was examined using FTIR spectroscopy. The FTIR
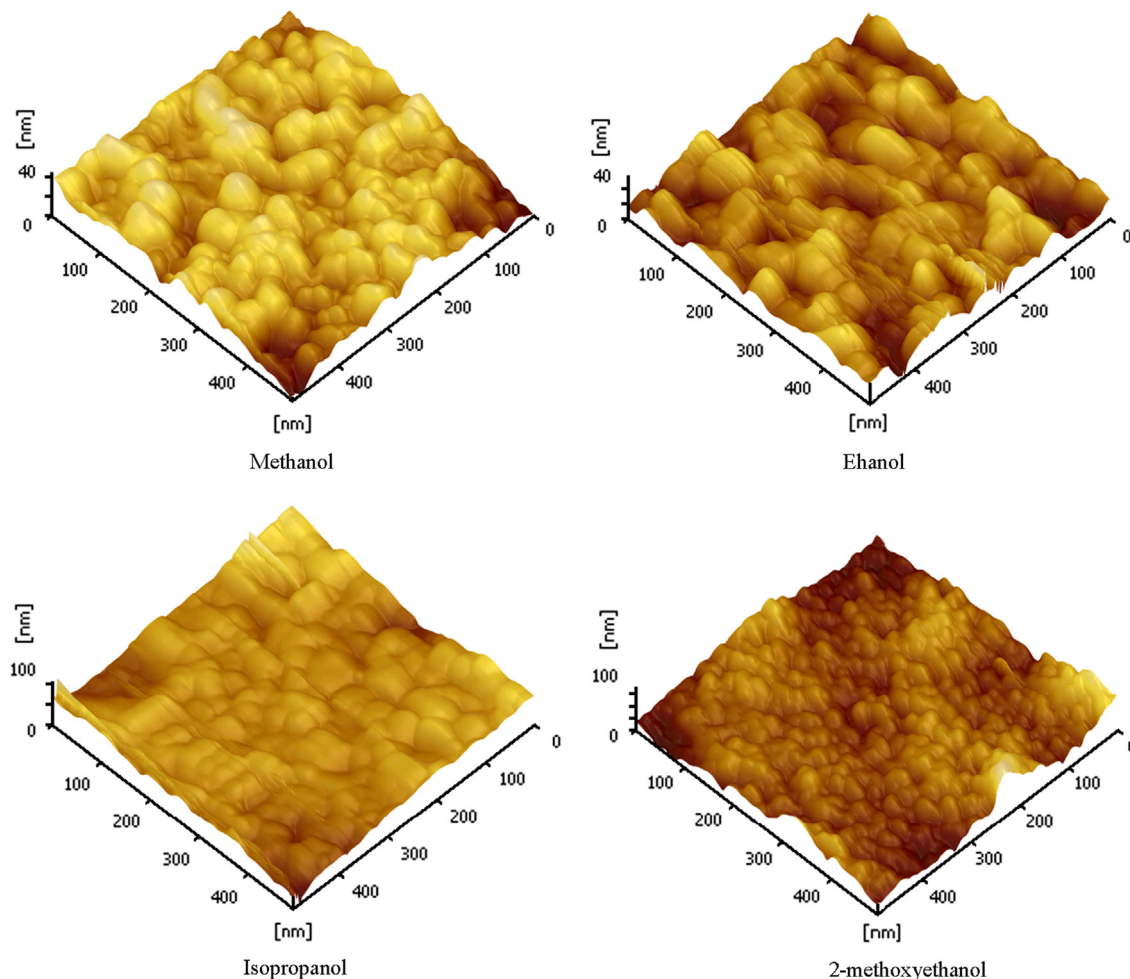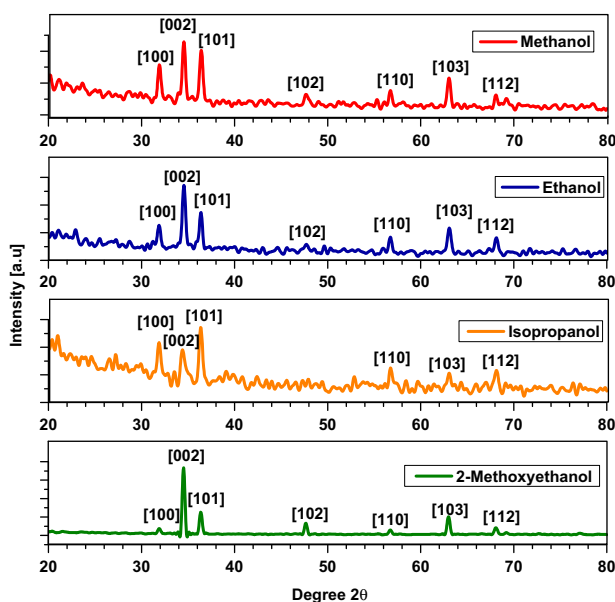
Fig. 4. 3-D view of ZnO thin films.

Fig. 5. X-ray diffraction patterns of ZnO thin films with various solvents used.

absorption spectrum of ZnO thin films deposited on SiO_2/Si substrate is shown in Fig. 6. The scanned absorption regions ranged from $400\,cm^{-1}$ to $2000\,cm^{-1}$, which represent the fingerprint of the materials [40]. The spectrum consists of 4 significant peaks, and all ZnO thin films prepared using different solvents contained the same peaks. The sharp peak located around $1092\,cm^{-1}$ corresponds to the stretching vibration of the Si–O mode of SiO_2 [41]. The band around $818\,cm^{-1}$ is assigned to v_2 (CO_3^{2-}) mode [28]. The absorption spectra around $618\,cm^{-1}$ is attributed to the existence of the local vibration of the substitution carbon in the Si crystal lattice [42]. The fourth sharp and intense absorption peak at $460\,cm^{-1}$ is attributed to the absorption spectra of Zn–O groups [43]. This absorption peak indicates that all the synthesized ZnO thin films displayed a symmetric stretching mode of hexagonal wurtzite structure [44].

Fig. 7 shows the optical transmittance spectra of ZnO thin films synthesized using different solvents. All ZnO thin films synthesized using different solvents exhibit good transparency in the visible region, with optical transmittance higher than 90%. By contrast, the MeOH-derived films exhibit average transmittance of only 80%. According to T.Y. Hill [45], the boiling point of the solvent is a causative factor that affects the optical transparency of the films; thus, a higher boiling point resulted in more optically transparent films. The boiling point of MeOH is lower compared with those of EtOH, IPA, and 2-ME solvents. The particles agglomerate instantaneously, and

the film shows low transmittance due to the low boiling point. As a result, ZnO thin films synthesized with EtOH, IPA, and 2ME are more transparent compared with MeOH solvent.

The absorption coefficient (α) for direct transition of ZnO films was determined using [46]

$$\alpha = \frac{\ln(1/T)}{d} \qquad (4)$$

where T represents the transmittance of ZnO films and d represents the film thickness. The optical band gap ($\alpha h v$) dependence on absorption coefficient (α) over the energy range of 3–3.5 eV at room temperature was calculated using the following equation [47]:

$$\alpha h v = B(h v - E_g)^n \qquad (5)$$

where $h v$ is photon energy, B is constant, E_g is the band gap energy, and n is the allowed direct band with a value of 1/2. The direct band gap energies for the different solvents used can be determined by plotting Tauc graphs, which is the curve of $(\alpha h v)^2$ vs. photo-energy ($h v$). This method was used to measure the different energies between the valence band and conduction band. The direct band gap of ZnO films is the interception between the tangent to the linear portion of the curve and the $h v$-axis shown in Fig. 8. The optical band gaps determined from the curves are summarized in Table 3. The result indicates that MeOH has the lowest band gap (3.25 eV), which is assumed to have better conductivity property. IPA and 2-ME have the highest band gap (3.28 eV). The variability in the band gap values in different solvents can be attributed to the microstructure and morphologies of the film surface, which would change the inter-atomic bond of the films [48]. All films show lower band gap compared with that of bulk ZnO (3.37 eV).

Many attempts have been made to relate the refractive index and the energy gap E_g through simple relationships [49–52]. However, these relations of n are independent of temperature and incident photon energy. In this paper, the various relations between n and E_g will be reviewed. Ravindra et al. [52] presented a linear form of n as a function of E_g:

$$n = \alpha + \beta E_g \qquad (6)$$

where $\alpha = 4.048$ eV^{-1} and $\beta = -0.62$ eV^{-1}. Light refraction and dispersion will be inspired. Herve and Vandamme [53] proposed an empirical relation as follows;

$$n = \sqrt{1 + \left(\frac{A}{E_g + B}\right)^2} \qquad (7)$$

where $A = 13.6$ eV and $B = 3.4$ eV. For group IV semiconductors, Ghosh et al. [54] published an empirical relationship based on the band structure and quantum dielectric considerations of Penn [55] and Van Vechten [56];

$$n^2 - 1 = \frac{A}{(E_g + B)^2} \qquad (8)$$

where $A = 25E_g + 212$ eV, $B = 0.21E_g + 4.25$ eV, and $(E_g + B)$ refers to an appropriate average energy gap of the material.
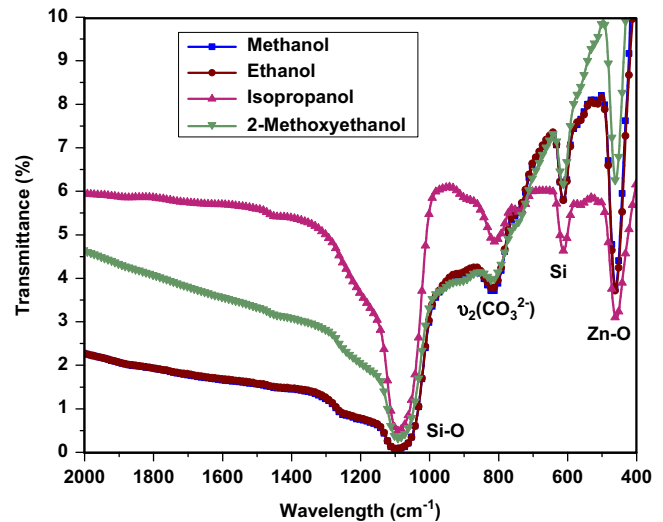

Fig. 6. FTIR absorption spectrum of ZnO thin films with sol–gel method.
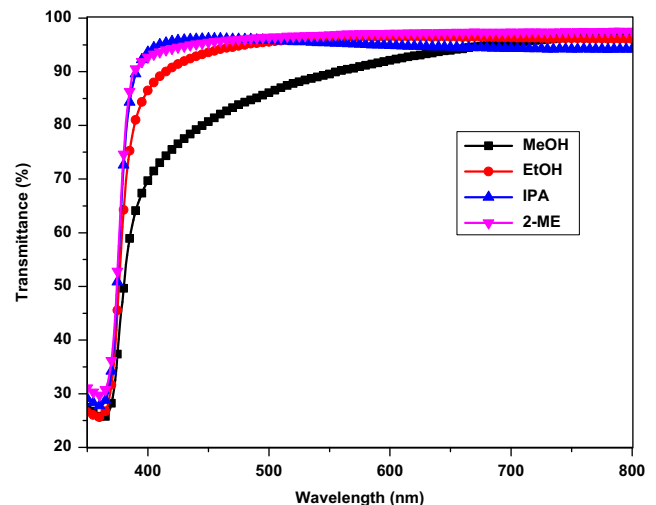

Fig. 7. Optical transmittance spectra of sol–gel derived ZnO thin films.

Table 2
Measured structural properties of ZnO thin films using XRD for different solvents.

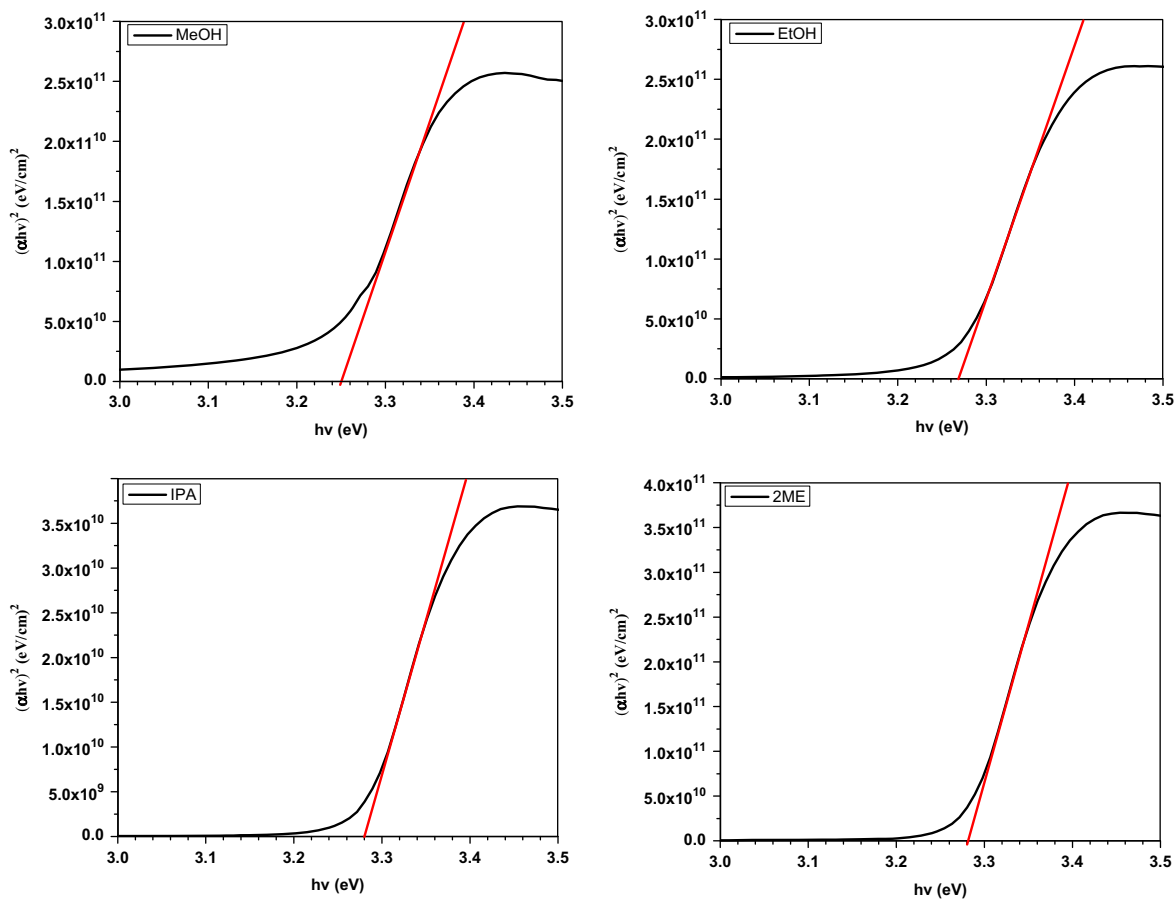| Solvent	XRD (100) peaks position	XRD (002) peaks position	Crystallite size (nm)	a (Å) (100)	c (Å) (002)
MeOH	31.92	34.56	21.64	3.23482	5.18648
EtOH	31.88	34.56	22.84	3.23877	5.18648
IPA	31.88	34.4	21.19	3.23877	5.20987
2ME	31.92	34.52	19.12	3.23482	5.19231

Fig. 8. Plot of $(\alpha h\nu)^2$ vs. the photon energy for different solvents derived ZnO thin films.

Table 3
Direct band-gap, and calculated refractive indices of ZnO thin films using Ravindra et al. [52], Herve and Vandamme [53] and Ghosh et al. [54] models corresponding to optical dielectric constant.

Solvent	Band-gap (eV)			n			ε_∞		
MeOH	3.25	3.39[a]	3.26[b]	2.033[f]	2.277[g]	2.319[h]	4.133[f]	5.182[g]	5.380[h]
EtOH	3.27	3.26[c]	3.11[d]	2.021[f]	2.271[g]	2.316[h]	4.083[f]	5.157[g]	5.362[h]
IPA	3.28	3.27[c]	3.28[d]	2.014[f]	2.268[g]	2.314[h]	4.058[f]	5.145[g]	5.352[h]
2-ME	3.28	3.22[c]	3.22[e]	2.014[f]	2.268[g]	2.314[h]	4.058[f]	5.145[g]	5.352[h]

[a]Singh et al. [57].
[b]Shah [58].
[c]Tsay et al. [31].
[d]Absalan and Ghodsi [59].
[e]Kashifet al. [60].
[f]Ravindra et al. [52].
[g]Herve and Vandamme [53].
[h]Ghosh et al. [54].

The calculated refractive indices of the end-point compounds and energy gaps are listed in Table 3; they are in good agreement with the experimental values [31,57–60].

This result is verified by the calculation of the optical dielectric constant ε_∞, which depends on the refractive index. Note that the optical dielectric constant $\varepsilon_\infty = n^2$ [61]. Our calculated refractive index values are in accordance to the experimental value shown in Table 3, which provide an appropriate model of Herve and Vandamme for solar cell applications.

4. Conclusions

ZnO thin films were successfully deposited through a sol–gel spin-coating process by utilizing different solvents. The

optical properties of the ZnO thin film were highly dependent on the surface roughness and grain size of the films. Therefore, compared with other solvents, ZnO thin films synthesized using 2-ME displayed lower surface roughness, finer grain size, higher transmittance in the visible range, higher crystallite quality, and larger band gap. The narrow peak of the XRD pattern indicated that all of the ZnO thin films had polycrystal-line hexagonal structures.

Acknowledgments

References

[1] S.M. Usman Ali, O. Nur, M. Willander, B. Danielsson, A fast and sensitive potentiometric glucose microsensor based on glucose oxidase coated ZnO nanowires grown on a thin silver wire, Sensors and Actuators B: Chemical 145 (2) (2010) 869–874.

[2] A. Fulati, S.M.U. Ali, M.H. Asif, N.u.H. Alvi, M. Willander, C. Brännmark, P. Strålfors, S.I. Börjesson, F. Elinder, B. Danielsson, An intracellular glucose biosensor based on nanoflake ZnO, Sensors and Actuators B: Chemical 150 (2) (2010) 673–680.

[3] G. Chai, O. Lupan, L. Chow, H. Heinrich, Crossed zinc oxide nanorods for ultraviolet radiation detection, Sensors Actuators A: Physical 150 (2) (2009) 184–187.

[4] H. Guo, J. Zhou, Z. Lin, ZnO nanorod light-emitting diodes fabricated by electrochemical approaches, Electrochemistry Communcations 10 (1) (2008) 146–150.

[5] D. Barreca, D. Bekermann, E. Comini, A. Devi, R.A. Fischer, A. Gasparotto, C. Maccato, G. Sberveglieri, E. Tondello, 1D ZnO nano-assemblies by Plasma-CVD as chemical sensors for flammable and toxic gases, Sensors and Actuators B: Chemical 149 (1) (2010) 1–7.

[6] M. Kashif, M.E. Ali, S.M.U. Ali, U. Hashim, Sol–gel synthesis of Pd doped ZnO nanorods for room temperature hydrogen sensing applica-tions, Ceramics International 39 (6) (2013) 6461–6466.

[7] E. Guillen, E. Azaceta, L.M. Peter, A. Zukal, R. Tena-Zaera, J.A. Anta, ZnO solar cells with an indoline sensitizer: a comparison between nanoparticulate films and electrodeposited nanowire arrays, Energy and Environmental Science 4 (9) (2011) 3400–3407.

[8] K. Matsubara, P. Fons, K. Iwata, A. Yamada, K. Sakurai, H. Tampo, S. Niki, ZnO transparent conducting films deposited by pulsed laser deposition for solar cell applications, Thin Solid Films 431–432 (2003) 369–372.

[9] M. Purica, E. Budianu, E. Rusu, Heterojunction with ZnO polycrystalline thin films for optoelectronic devices applications, Microelectronic Engi-neering 51–52 (0) (2000) 425–431.

[10] M.H. Huang, Y. Wu, H. Feick, N. Tran, E. Weber, P. Yang, Catalytic growth of zinc oxide nanowires by vapor transport, Advanced Materials 13 (2) (2001) 113–116.

[11] M. Kashif, S.M. Usman Ali, M.E. Ali, H.I. Abdulgafour, U. Hashim, M. Willander, Z. Hassan, Morphological, optical, and Raman character-istics of ZnO nanoflakes prepared via a sol–gel method, Physica Status Solidi A 209 (1) (2012) 143–147.

[12] M. Kashif, U. Hashim, S.M.U. Ali, A.S. Ala'eddin, M. Willander, M.E. Ali, Structural and impedance spectroscopy study of Al-doped ZnO nanorods grown by sol–gel method, Microelectronics International 29 (3) (2012) 131–135.

[13] Y.B. Li, Y. Bando, T. Sato, K. Kurashima, ZnO nanobelts grown on Si substrate, Applied Physics Letters 81 (1) (2002) 144–146.

[14] W.L. Hughes, Z.L. Wang, Controlled synthesis and manipulation of ZnO nanorings and nanobows, Applied Physics Letters 86 (4) (2005) 043106 - 043106-3.

[15] S. Kim, M.C. Jeong, B.Y. Oh, W. Lee, J.-M. Myoung, Fabrication of Zn/ZnO nanocables through thermal oxidation of Zn nanowires grown by RF magnetron sputtering, Journal of Crystal Growth 290 (2) (2006) 485–489.

[16] S.M.U. Ali, M. Kashif, Z.H. Ibupoto, M. Fakhar-e-Alam, U. Hashim, M. Willander, Functionalised zinc oxide nanotube arrays as electroche-mical sensors for the selective determination of glucose, Micro and Nano Letters 6 (8) (2011) 609–613.

[17] X. Ren, C.H. Jiang, D.D. Li, L. He, Fabrication of ZnO nanotubes with ultrathin wall by electrodeposition method, Materials Letters 62 (17-18) (2008) 3114–3116.

[18] J.Y. Park, Y.S. Yun, Y.S. Hong, H. Oh, J.-J. Kim, S.S. Kim, Synthesis and electrical properties of aligned ZnO nanocolumns, Composites Part B: Engineering 37 (6) (2006) 408–412.

[19] Y. Yang, B.K. Tay, X.W. Sun, Z.J. Han, Z.X. Shen, C. Lincoln, T. Smith, Effective photoluminescence modification of ZnO nanocombs by plasma immersion ion implantation, in: Proceedings of the 2nd IEEE International Nanoelectronics Conference, INEC 2008, 2008, pp. 20–24.

[20] J. Zhang, Y. Yang, F. Jiang, J. Li, Fabrication, structural characterization and the photoluminescence properties of ZnO nanoneedle arrays, Physica E 27 (1–2) (2005) 302–307.

[21] M. Dutta, S. Mridha, D. Basak, Effect of sol concentration on the properties of ZnO thin films prepared by sol–gel technique, Applied Surface Science 254 (9) (2008) 2743–2747.

[22] S.A. Kamaruddin, K.Y. Chan, H.K. Yow, M. Zainizan Sahdan, H. Saim, D. Knipp, Zinc oxide films prepared by sol–gel spin coating technique, Applied Physics A 104 (1) (2010) 263–268.

[23] B. Deng, X. Yan, Q. Wei, W. Gao, AFM characterization of nonwoven material functionalized by ZnO sputter coating, Materials Characteriza-tion 58 (10) (2007) 854–858.

[24] J.L. Yang, S.J. An, W.I. Park, G.C. Yi, W. Choi, Photocatalysis using ZnO thin films and nanoneedles grown by metal–organic chemical vapor deposition, Advanced Materials 16 (18) (2004) 1661–1664.

[25] L. Wang, X. Zhang, S. Zhao, G. Zhou, Y. Zhou, J. Qi, Synthesis of well-aligned ZnO nanowires by simple physical vapor deposition on c-oriented ZnO thin films without catalysts or additives, Applied Physics Letters 86 (2) (2005) 024103–024108.

[26] A. Ashour, M.A. Kaid, N.Z. El-Sayed, A.A. Ibrahim, Physical properties of ZnO thin films deposited by spray pyrolysis technique, Applied Surface Science 252 (22) (2006) 7844–7848.

[27] W. Shen, Y. Zhao, C. Zhang, The preparation of ZnO based gas-sensing thin films by ink-jet printing method, Thin Solid Films 483 (1-2) (2005) 382–387.

[28] T. Sahoo, M. Kim, M.H. Lee, L.W. Jang, J.W. Jeon, J.S. Kwak, I.Y. Ko, I.H. Lee, Nanocrystalline ZnO thin films by spin coating-pyrolysis method, Journal of Alloys and Compounds 491 (1-2) (2010) 308–313.

[29] L. Znaidi, G. SolerIllia, S. Benyahia, C. Sanchez, A. Kanaev, Oriented ZnO thin films synthesis by sol–gel process for laser application, Thin Solid Films 428 (1) (2003) 257–262.

[30] M. Alam, D. Cameron, Characterization of transparent conductive ITO thin films deposited on titanium dioxide film by a sol–gel process, Surface and Coatings Technology 142 (2001) 776–780.

[31] C.-Y. Tsay, K.-S Fan, Y.-W Wang, C.-J Chang, Y.-K Tseng, C.-K Lin, Transparent semiconductor zinc oxide thin films deposited on glass substrates by sol–gel process, Ceramics International 36 (6) (2010) 1791–1795.

[32] M. Popa, R.A. Mereu, M. Filip, M. Gabor, T. Petrisor Jr, L. Ciontea, T. Petrisor, Highly c-axis oriented ZnO thin film using 1-propanol as solvent in sol–gel synthesis, Materials Letters 92 (0) (2013) 267–270.

[33] S. Flickyngerova, K. Shtereva, V. Stenova, D. Hasko, I. Novotny, V. Tvarozek, P. Sutta, E. Vavrinsky, Structural and optical properties of sputtered ZnO thin films, Applied Surface Science 254 (12) (2008) 3643–3647.

[34] N. Shakti, P. Gupta, Structural and optical properties of sol–gel prepared ZnO thin film, Applied Physics Research 2 (1) (2010) P19.

[35] S.A. Kamaruddin, Y.C. Kah, K.Y. Ho, M.Z. Sahdan, H. Saim, D. Knipp, Zinc oxide films prepared by sol–gel spin coating technique, Applied Physics A 104 (1) (2011) 263–268.

[36] B.D. Cullity, S.R. Stock, in: Elements of X-ray Diffraction, 3rd edition, Prentice Hall, 2001.

[37] H. Metin, R. Esen, Annealing effects on optical and crystallographic properties of CBD grown CdS films, Semiconductor Science and Technology 18 (7) (2003) 647.

[38] S.J. Pearton, D.P. Norton, K. Ip, Y.W. Heo, T. Steiner, Recent advances in processing of ZnO, Journal of Vaccum Science and Technology B 22 (3) (2004) 932–948.

[39] C. Suryanarayana, G. Norton, X-ray Diffraction: A Practical Approach, Springer, 1998.

[40] L. Feng, A. Liu, Y. Ma, M. Liu, B. Man, Fabrication, structural characterization and optical properties of the flower-like ZnO nanowires, Acta Physica Polonica A 117 (3) (2010) 512–517.

[41] N. Laidani, R. Capelletti, M. Elena, L. Guzman, G. Mariotto, A. Miotello, P.M. Ossi, Spectroscopic characterization of thermally treated carbon-rich $Si_{1-x}C_x$ films, Thin Solid Films 223 (1) (1993) 114–121.

[42] Y. Sun, T. Miyasato, J.K. Wigmore, Characterization of excess carbon in cubic SiC films by infrared absorption, Journal of Applied Physics 85 (6) (1999) 3377–3379.

[43] P. Singh, A. Kumar, D.Kaur Deepak, Growth and characterization of ZnO nanocrystalline thin films and nanopowder via low-cost ultrasonic spray pyrolysis, Journal of Crystal Growth 306 (2) (2007) 303–310.

[44] S. Rasouli, S.J. Moeen, A.M. Arabi, Synthesis of wurtzitenano-crystalline ZnO–CoO pigment by high energy milling, Progress in Color, Colorants and Coatings 2 (2009) 45–51.

[45] T.Y. Hill, Fabrication of zinc oxide thin films for renewable energy and sensor applications, thesis, Wright State University, 2010.

[46] W.-n. Miao, X.-f. Li, Q. Zhang, L. Huang, Z.-j. Zhang, L. Zhang, X.-j. Yan, Transparent conductive In_2O_3:Mo thin films prepared by reactive direct current magnetron sputtering at room temperature, Thin Solid Films 500 (1) (2006) 70–73.

[47] S. Singh, H. Kaur, D. Pathak, R. Bedi, Zinc oxide nanostructures as transparent window layer for photovoltaic application, Dig. J. Nanomater. Bios. 6 (2011) 689-698.

[48] N. Samaele, P. Amornpitoksuk, S. Suwanboon, Effect of pH on the morphology and optical properties of modified ZnO particles by SDS via a precipitation method, Powder Technology 203 (2) (2010) 243–247.

[49] T. Moss, A relationship between the refractive index and the infra-red threshold of sensitivity for photoconductors, Proceedings of the Physical Society Section B 63 (3) (2002) 167.

[50] V.P. Gupta, N.M. Ravindra, Comments on the Moss formula, Physica Status Solidi B 100 (2) (1980) 715–719.

[51] P. Hervé, L.K.J. Vandamme, General relation between refractive index and energy gap in semiconductors, Infrared Physics and Technology 35 (4) (1994) 609–615.

[52] N.M. Ravindra, S. Auluck, V.K. Srivastava, On the Penn Gap in semiconductors, Physica Status Solidi B 93 (2) (1979) K155–K160.

[53] P.J.L. Herve, L.K.J. Vandamme, Empirical temperature dependence of the refractive index of semiconductors, Journal of Applied Physics. 77 (10) (1995) 5476–5477.

[54] D. Ghosh, L. Samanta, G. Bhar, A simple model for evaluation of refractive indices of some binary and ternary mixed crystals, Infrared Physics 24 (1) (1984) 43–47.

[55] D.R. Penn, Wave-number-dependent dielectric function of semiconductors, Physical Review 128 (5) (1962) 2093–2097.

[56] J.A. Van Vechten, Quantum dielectric theory of electronegativity in covalent systems. I. electronic dielectric constant, Physical Review 182 (3) (1969) 891–905.

[57] A. Singh, R. Kumar, N. Malhotra, Suman, Preparation of ZnO nano-particles by solvothermal process, International Journal for Science and Emerging Technologies with Latest Trends 4 (1) (2012) 49–53.

[58] M.A. Shah, Formation of zinc oxide nanoparticles by the reaction of zinc metal with methanol at very low temperature, African Physics Review 2 (2008) 106–109.

[59] H. Absalan, F. EsmaieliGhodsi, Comparative study of ZnO thin films prepared by different sol–gel route, Iranian Journal of Physics Research 11 (4) (2012) 423–428.

[60] M. Kashif, Y. Al-Douri, U. Hashim, M.E. Ali, S.M.U. Ali, M. Willander, Characterisation, analysis and optical properties of nanostructure ZnO using the sol–gel method, Micro and Nano Letters 7 (2) (2012) 163–167.

[61] G.A. Samara, Temperature and pressure dependences of the dielectric constants of semiconductors, Physical Review B 27 (6) (1983) 3494–3505.